## ROYAL SOCIETY OF CHEMISTRY

### **Journal Name**

### **FULL PAPER**

# Thermodynamics of Pillararene Guest Complexation: Blinded Dataset for the SAMPL9 Challenge

Received 00th January 20xx, Accepted 00th January 20xx

Chun-Lin Deng, Ming Cheng, Peter Y. Zavalij, and Lyle Isaacs\*

DOI: 10.1039/x0xx00000x

www.rsc.org/

We report an investigation of the complexation between a water soluble pillararene host (WP6) and a panel of hydrophobic cationic guests (G1 – G20) by a combination of  $^1\text{H}$  NMR spectroscopy and isothermal titration calorimetry in phosphate buffered saline. We find that WP6 forms 1:1 complexes with  $K_a$  values in the  $10^4-10^9$   $M^{-1}$  range driven by favorable enthalpic contributions. This thermodynamic dataset serves as blinded data for the SAMPL9 challenge.

### Introduction

A crucial step in the drug development process is the discovery and optimization of small molecule ligands that bind to their target proteins in aqueous solution. Experimentally, this process is very expensive and time consuming because it requires an iterative process of chemical synthesis and the measurement of binding affinity.1 Accordingly, the development of computational methods that successfully rank ligands by relative affinity and deliver binding free energies with errors below 1 kcal mol-1 are highly sought by the computational chemistry community and pharmaceutical industry. Validation is an important step in the development of such computational methods. However, testing of new methods on protein•ligand systems can be computationally expensive and time consuming because proteins are large and complex entities which require that extensive conformational sampling to ensure convergence. To address this issue, a group of computational chemists has organized a series of Statistical Assessment of the Modeling of Proteins and Ligands (SAMPL) challenges<sup>2</sup> to assess and improve the state-of-the-art. Over the years, SAMPL challenges relied upon unpublished blinded datasets including small molecule solvation free energies, HIV integrase inhibitors binding free energy, and pKa and octanolwater partition coefficient predictions.3 Supramolecular chemists are also deeply involved in the fundamentals and applications of host•guest binding and measurement of the binding free energies.<sup>4</sup> Given that supramolecular hosts are typically smaller and conformationally more homogenous than proteins and that some supramolecular systems achieve binding affinities and selectivities that rival Nature suggested that host•guest systems (Figure 1) should be included in the SAMPL challenges.<sup>5</sup>

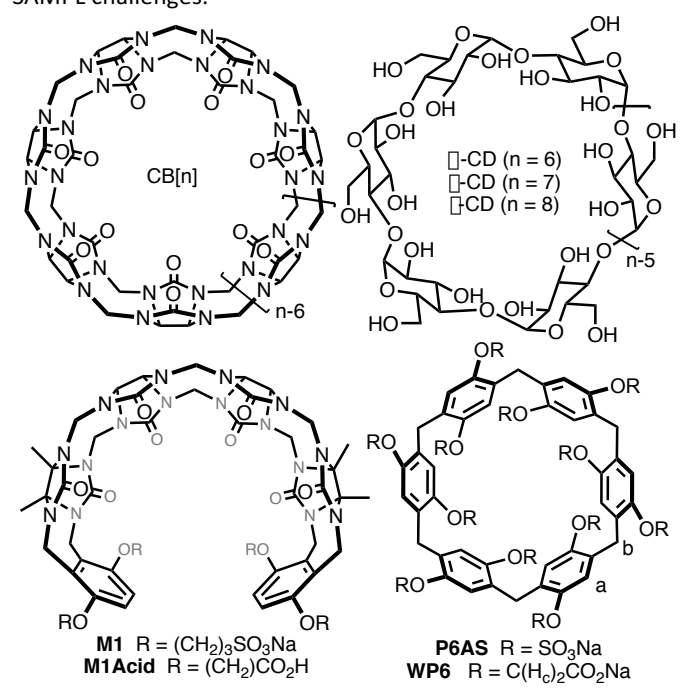


Figure 1. Structures of (acyclic) CB[n], cyclodextrins, and pillararenes.

The Isaacs group has a longstanding interest in the cucurbit[n]uril (CB[n]) family of molecular containers and has been involved in the elucidation of the mechanism of CB[n] formation as a means to create new CB[n]-type receptors and in the delineation of their host guest recognition properties. We discovered that CB[n] bind tightly and with high selectivity toward hydrophobic cations in water (Ka typically  $10^6 - 10^{12} \, \text{M}^{-1}$ ). 8 The origin of the tight binding was traced to the presence

Department of Chemistry and Biochemistry, University of Maryland, College Park, Maryland 20742, USA. E-mail: <a href="mailto:Lisaacs@umd.edu">Lisaacs@umd.edu</a>.

 $<sup>^\</sup>dagger$  Electronic Supplementary Information (ESI) available: Details of synthesis, NMR, and ITC experiments. See DOI: 10.1039/x0xx00000x

of intracavity waters that lack a full complement of H-bonds that are released upon complexation.9 We, and others, have used CB[n]-type receptors as in vivo sequestration agents and for (targeted) drug delivery applications.<sup>5f, 10</sup> Since SAMPL3, the Isaacs group has provided unpublished Ka values for guests toward various CB[n]-type receptors (e.g. CB[n] (n = 7, 8), acyclic CB[n] (e.g. M1Acid), and glycoluril derived molecular clips).11 The groups of Bruce Gibb and Michael Gilson have supplied blinded datasets for deep cavity cavitands and cyclodextrin derivatives, respectively. 12 One issue the computational chemists encountered in previous SAMPL challenges with acyclic CB[n]-type receptors conformational sampling. Recently, we have become interested in the pillararene family<sup>13</sup> of molecular containers (e.g. WP6, P6AS) as sequestration agents. 5f, 14 Pillararenes are macrocyclic and display high affinity toward cationic guests like viologens in water which makes them ideally suited as an alternative scaffold for the SAMPL challenges.5c, 15 Herein, we describe the binding of WP615 - which is a water soluble derivative of pillar[6]arene - toward a series of hydrophobic cations which serves as a blinded dataset for the SAMPL9 challenge.

### **Results and Discussion**

This results and discussion section is organized as follows. First, we present the selection of the host (WP6) and guests (G1 – G20) used in the study. Subsequently, we present a qualitative investigation of the host•guest complexation by analysis of complexation induced changes in <sup>1</sup>H NMR chemical shift and multiplicity. Thereafter, we present the determination of host•guest binding affinity and enthalpy by isothermal titration calorimetry (ITC). Finally, we discuss the thermodynamic parameters as a function of guest structure and offer come conclusions.

### Selection of Host and Guests.

Previous SAMPL challenges have featured macrocyclic CB[7] and CB[8],<sup>2b, 11b, 11f</sup> glycoluril derived molecular clips and acyclic CB[n] that feature carboxylate or sulfonate groups,11a, c, e deep cavity cavitands, 12a, b and cyclodextrins. 12c In previous challenges, issues relating to the conformational flexibility of acyclic CB[n] hosts and the degree of deprotonation of ionizable functional groups have arisen. Accordingly, for SAMPL9 challenge we decided to select WP6 as host because it is more defined conformationally and is known to undergo strong host • guest complexation in water. 14b, 15 Most studies of host • guest complexation of WP6 use less competitive media (e.g. unbuffered water or buffered water). To make the SAMPL9 challenge more biologically relevant, we elected to perform our studies in phosphate buffered saline (PBS) at physiological pH (pH 7.4). Given that WP6 is anionic at neutral pH, we knew that binding of cationic guests would be favored. Accordingly, we selected guests G1 - G20 (Figure 2) which are mono- and diammonium ions which were available from our previous studies of CB[n] • guest complexation events.8, 11b, 11d, 16 Guests G1 - G20 feature different numbers of cationic residues, different alkylation states (e.g.  $1^{\circ}$ ,  $2^{\circ}$ ,  $3^{\circ}$ ,  $4^{\circ}$ ), and different sized hydrophobic residues. Given that **WP6** is highly negatively charged at neutral pH, we expected that **G1** – **G20** would form **WP6•G** complexes whose  $K_a$  values would span several orders of magnitude thereby making it easier for the computationalists to predict changes in binding free energy as a function of guest structure.

**Figure 2.** Structures of guests **G1** – **G20** used in this study. Panel a) guests studied by <sup>1</sup>H NMR and ITC, b) guests studied only by <sup>1</sup>H NMR.

### Qualitative <sup>1</sup>H NMR Host•Guest Recognition Study

As drawn in Figure 1, WP6 features a  $C_6$ -axis and overall  $D_6$ symmetry and is therefore chiral. 13b However, because the  $OCH_2CO_2Na$  substituents can rotate through the annulus of the macrocycle WP6 is isolated as a racemic mixture of planar chiral macrocycles (e.g.  $R_p$  and  $S_p$ ).<sup>17</sup> Figure 3a shows the <sup>1</sup>H NMR spectrum recorded for WP6 which features a single sharp resonance for  $H_a$ ,  $H_b$ , and  $H_c$  on the chemical shift timescale. This observation strongly suggests that rotation through the annulus is fast on the chemical shift timescale. Initially, we studied the binding of WP6 toward the panel of guests (G1 - G20) in  $D_2O$  by  $^1H$ NMR stoichiometry at 1:1 and 1:2 WP6:guest stoichiometry (Supporting Information). The <sup>1</sup>H NMR spectra recorded for WP6, G1, and 1:1 and 1:2 mixtures of WP6 and G1 (Figure 3) illustrate the spectral changes that are commonly observed. For example, at a 1:1 WP6:G1 stoichiometry (Figure 3c), the resonances for G1 within the WP6•G1 complex undergo substantial upfield shifts due to their location in the magnetically shielding environment of the Journal Name FULL PAPER

macrocyclic cavity defined by the aromatic walls. Conversely, host resonance Ha undergoes a smaller downfield shift which can be explained by changes in the orientation of the aromatic walls with respect to each other. More interestingly, the H<sub>c</sub> resonance of the OCH<sub>2</sub>CO<sub>2</sub>Na groups with the WP6•G1 complex shift downfield and split into an AB quartet (H<sub>c</sub>, H<sub>c'</sub>) for the diastereotopic methylene groups. In combination, this indicates that rotation through the annulus is slow on the chemical shift timescale for WP6•G1 but that exchange of guest G1 is fast on the chemical shift timescale which renders the top and bottom portals of WP6 equivalent. Figure 3d shows the <sup>1</sup>H NMR spectrum recorded at a 1:2 WP6:G1 stoichiometry. Compared to Figure 3c, the resonances for G1 shift back toward their locations for uncomplexed G1 which further confirms the fast exchange of G1 on the chemical shift timescale. The  $D_6$ -symmetric conformation of uncomplexed **WP6** in dominant However, pillararenes are capable of in aqueous solution. conformational diastereoisomerism when one or more of the aromatic rings flips. For example, in the case of the WP6•G13 complex we observe a dramatic increase in complexity in the 5.5 -7.5 ppm region of the spectrum which is consistent with reduced symmetry of the complexes (Supporting Information, Figure S12).

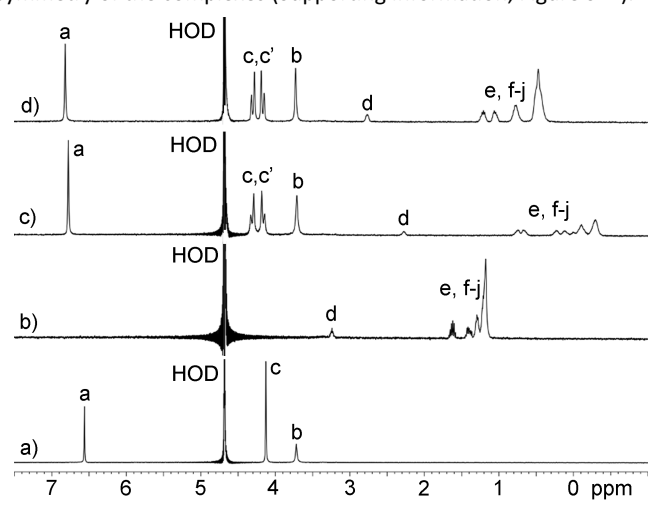


Figure 3.  $^{1}$ H NMR spectra recorded (400 MHz, RT, D<sub>2</sub>O) for: a) WP6 (1 mM), b) G1 (1 mM), c) a mixture of WP6 (1 mM) and G1 (1 mM), and d) a mixture of host WP6 (1 mM) and G1 (2 mM).

The <sup>1</sup>H NMR spectra recorded for mixtures of **WP6** and guest **G14** (Figure 4) provide a beautiful example of stereochemistry and chemical exchange in host • guest chemistry. For example, the observation of a sharp singlets for WP6 (Figure 4a) indicates that the top and bottom portals of WP6 are equivalent due to the presence of a  $C_6$ -axis and six perpendicular  $C_2$ -axes resulting in  $D_6$  point group symmetry. Similarly, the adamantane residue of guest G14 has a  $C_3$ -axis and three mirror planes which results in single resonances for  $H_m$  and  $H_n$ , whereas  $H_o$  and  $H_p$  are part of the diastereotopic CH<sub>2</sub>-group (Figure 4b). The protons on the N-CH<sub>2</sub>CH<sub>2</sub>-N group (H<sub>k</sub> and H<sub>l</sub>) appear as coupled triplets as expected. The situation changes completely within the WP6•G14 complex (Figure 4c). As can be seen (Figure 4a,c), the aromatic resonance H<sub>a</sub> splits into two singlets (H<sub>a</sub>, H<sub>a'</sub>). Apparently, the WP6•G14 complex undergoes slow guest exchange which renders the top and bottom portals of the complex chemically distinct with different chemical shifts; complexation maintains the  $C_6$ -axis but eliminates the six perpendicular  $C_2$ -axes. The presence of four doublets for H<sub>c</sub> (H<sub>c</sub> - H<sub>c"'</sub>) for WP6•G14 reflects the top-bottom dissymmetry and that this CH<sub>2</sub>-group is diastereotopic within the overall chiral and racemic complex. Figure 5 shows an MMFF minimized molecular model of WP6•G14 which illustrates these symmetry considerations. Even more interesting is the appearance of the resonances for guest  $\mathbf{G14}$  within the  $\mathbf{WP6} \bullet \mathbf{G14}$  complex. For example,  $H_k$  and  $H_l$  split into four resonances  $H_l$ ,  $H_l$ ,  $H_k$ ,  $H_k$ , because the chiral WP6•G14 complex renders these CH<sub>2</sub>-groups diastereotopic and all four protons are chemically distinct. Protons Hn still appear as a single resonance in WP6•G14 because the C<sub>3</sub>-axis present in G14 is maintained in the WP6•G14 complex. Even more interesting is that the six protons H<sub>m</sub> that appear as a single resonance in G14 split into a pair of coupled doublets H<sub>m</sub> and  $H_{m'}$  within WP6•G14. The three mirror planes that are present in the adamantane skeleton of G14 are destroyed upon complexation to form the chiral WP6•G14 complex which renders these three CH2-groups diastereotopic. All of the protons of guest G14 experience a large upfield shift upon complexation which reflects their complexation inside the hydrophobic magnetically shielding environment of the WP6 cavity. At a 1:2 WP6:G14 stoichiometry the guest exchange rate increases which results in averaged NMR where the ethylene diammonium ion tail can point out of either portal which results in a merging of the Ha and Ha' resonances as well as the  $H_c$  –  $H_{c^{\prime\prime\prime}}$  resonances as expected based on symmetry considerations. The guest resonances also merge and shift back toward the chemical shift for uncomplexed G14 as expected.

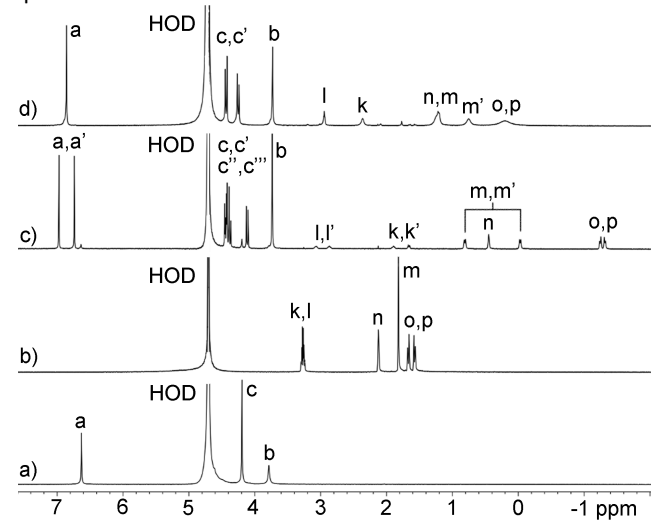
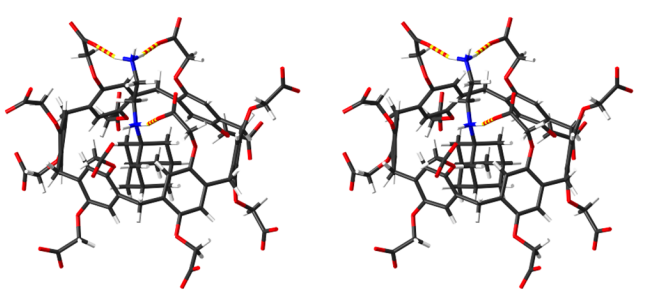
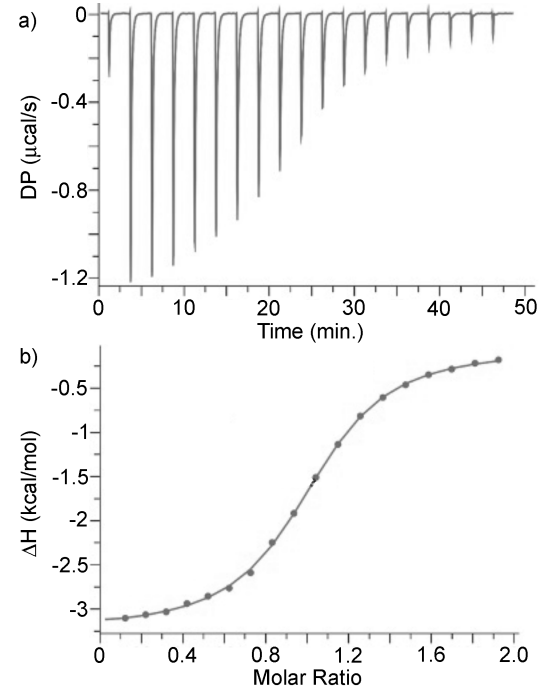


Figure 4.  $^{1}$ H NMR spectra recorded (600 MHz, RT,  $D_2O$ ) for: a) **WP6** (1 mM), b) **G14** (1 mM), c) a mixture of **WP6** (1 mM) and **G14** (1 mM), and d) a mixture of host **WP6** (1 mM) and **G14** (2 mM).



**Figure 5.** Cross-eyed stereoview of an MMFF minimized model of **WP6•G14**. Color code: C, gray; H, white; N, blue; O, red; H-bonds, red-yellow striped.



**Figure 6.** a) ITC thermogram recorded during the direct titration of **WP6** (200  $\mu$ M) in the cell with **G7** (2.0 mM) in the syringe, b) Fitting of the data to a 1:1 binding model with  $K_0 = 1.31 \times 10^5$  M<sup>-1</sup>.

### Measurement and Discussion of the Thermodynamic Parameters of Complex Formation.

After having qualitatively assessed the binding properties of WP6 toward the guest panel by <sup>1</sup>H NMR spectroscopy we decided to measure the thermodynamic parameters of complexation. Given that WP6 is known to display tight binding and our desire to use a single analytical method across our measurements we turned to isothermal titration calorimetry (ITC) measurements which allows accurate Ka determination over a wide dynamic range. 18 Figure 6a shows the thermogram measured when WP6 (200  $\mu$ M) in the ITC cell was titrated with a solution of G7 (2.0 mM) in the syringe. All ITC experiments were conducted in duplicate. Figure 6b shows the fitting of the integrated heat values to a 1:1 binding model implemented in the PEAQ ITC data analysis software with K<sub>a</sub> =  $1.31 \times 10^5$  M<sup>-1</sup> and  $\Delta H$  = -3.18 kcal mol<sup>-1</sup>. The K<sub>a</sub> and  $\Delta H$  values for the weaker complexes ( $K_a \le 5 \times 10^6 \text{ M}^{-1}$ ) were determined in an analogous manner by direct ITC titrations and are presented in Table 1. In these direct titrations, the fixed concentration of WP6 in the cell was manipulated in order to optimize the c-value<sup>18c</sup> and therefore sample a larger portion of the binding isotherm and therefore deliver more reliable results.

**Table 1.** Binding constants ( $K_0$ ,  $M^{-1}$ ) and enthalpies ( $\Delta H$ , kcal mol<sup>-1</sup>) measured for **WP6**•guest complexes. Conditions: 1x PBS buffer, pH 7.4, 298.15 K.

Guest	K <sub>a</sub> (M <sup>-1</sup> )	$\Delta$ H (kcal mol $^{-1}$ )
G1 <sup>a</sup>	$(5.29 \pm 0.07) \times 10^4$	-8.08 ± 0.02
G2 <sup>b</sup>	$(4.59 \pm 0.35) \times 10^7$	-6.10 ± 0.02
(±)-G3 <sup>a</sup>	(6.45 ± 0.18) × 10 <sup>5</sup>	-4.75 ± 0.02
G4 <sup>e</sup>	$(5.08 \pm 0.11) \times 10^4$	-4.15 ± 0.02
G5 <sup>f</sup>	$(9.01 \pm 0.23) \times 10^3$	-3.95 ± 0.03
G6 <sup>c</sup>	$(7.09 \pm 0.44) \times 10^5$	-6.90 ± 0.07
G7 <sup>d</sup>	$(1.31 \pm 0.05) \times 10^5$	-3.18 ± 0.02
G8 <sup>e</sup>	$(2.35 \pm 0.04) \times 10^4$	-9.55 ± 0.05
G9 <sup>f</sup>	(3.75 ± 0.31) × 10 <sup>4</sup>	-5.31 ± 0.08
<b>G10</b> <sup>b</sup>	$(1.61 \pm 0.08) \times 10^7$	-6.23 ± 0.02
<b>G11</b> <sup>f</sup>	$(3.37 \pm 0.05) \times 10^4$	-5.61 ± 0.02
(±)-G12 <sup>g</sup>	$(9.43 \pm 0.31) \times 10^7$	-7.45 ± 0.02
<b>G13</b> <sup>c</sup>	$(1.63 \pm 0.11) \times 10^6$	-4.98 ± 0.04
<b>G14</b> <sup>i</sup>	$(4.69 \pm 0.09) \times 10^9$	-16.4 ± 0.02
<b>G15</b> <sup>h</sup>	$(1.76 \pm 0.06) \times 10^7$	-7.03 ± 0.03
G16 <sup>e</sup>	$(1.32 \pm 0.03) \times 10^4$	-7.49 ± 0.06
<b>G17</b> <sup>a</sup>	$(2.29 \pm 0.06) \times 10^5$	-4.15 ± 0.02

Measured by direct ITC titration of **WP6** in the cell with guest in the syringe:  $^{a}$  [**WP6**] = 0.1 mM, [guest] = 1.0 mM;  $^{c}$  [**WP6**] = 0.05 mM, [guest] = 0.5 mM;  $^{d}$  [**WP6**] = 0.2 mM, [guest] = 2.0 mM;  $^{e}$  [**WP6**] = 0.5 mM, [guest] = 5.0 mM;  $^{f}$  [**WP6**] = 1.0 mM, [guest] = 10 mM. Measured by competitive ITC titration of a mixture of **WP6** (0.1 mM) and **G7** in the cell with guest (1 mM) in the syringe:  $^{b}$  [**G7**] = 0.2 mM;  $^{g}$  [**G7**] = 0.5 mM;  $^{h}$  [**G7**] = 1.0 mM.  $^{i}$  Measured by competitive ITC titration of a mixture of **WP6** (0.1 mM) and **G15** (0.5 mM) in the cell with guest (1 mM) in the syringe.

For the tighter binding complexes WP6•G2 and WP6•G12 with  $K_a > 10^7 M^{-1}$  we could not optimize the c-values by reducing the fixed concentration of WP6 in the cell and therefore turned to competitive ITC titrations. 18b In competitive ITC titrations the cell contains a solution of WP6 and an excess of a weaker binding guest into which a solution of the tighter binding guest is titrated. The integrated heat data from the competitive ITC titration is fitted to the competitive binding model implemented in the PEAQ ITC data analysis software using the known concentrations of host and weak binding guest along with the known  $\mbox{\ensuremath{K_a}}$  and  $\Delta\mbox{\ensuremath{H}}$  values for the host • weak guest complexes as inputs to extract the Ka and  $\Delta H$ values for the host • tight guest complex. Experimentally, it is important that the host-weak guest and host-tight guest complexes have significantly different  $\Delta H$  values otherwise the titration will not produce sufficient heat to allow a proper fitting of the data. Experimentally, we selected **G7** as the weak binding complex because its Ka toward WP6 is large enough to make it a reasonable competitor and the  $\Delta H$  for the WP6•G7 complex is significantly smaller than those of the other complexes. Figure 7a shows the thermogram recorded during

Journal Name FULL PAPER

the titration of a solution of **WP6** (100  $\mu$ M) and **G7** (0.2 mM) in the cell with **G2** (1 mM) in the syringe. Figure 7b shows the fitting of the integrated heat versus **WP6**:**G7** molar ratio to the competitive binding model that allowed us to determine  $K_a = 4.59 \times 10^7$  M<sup>-1</sup> and  $\Delta H = -6.10$  kcal mol<sup>-1</sup> for the tighter **WP6**•**G2** complex. Please note that the limiting  $\Delta H$  value at low molar ratio ( $\approx$  -3.2 kcal mol<sup>-1</sup>; Figure 7b) corresponds to the difference between the  $\Delta H$  values for the **WP6**•**G7** and **WP6**•**G2** complexes. The  $K_a$  and  $\Delta H$  values for the **WP6**•**G12**, **WP6**•**G14**, **WP6**•**G15** complexes were determined by an analogous competitive ITC titration (Supporting Information).

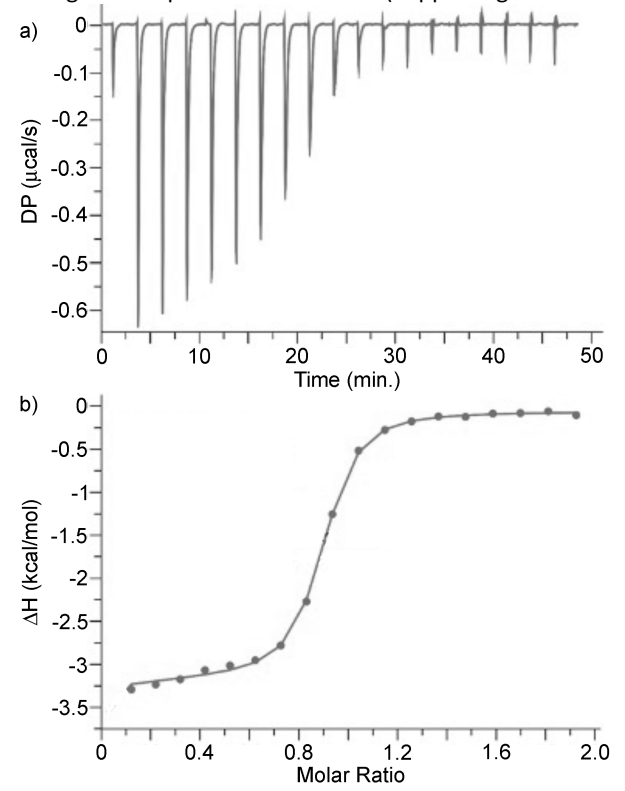
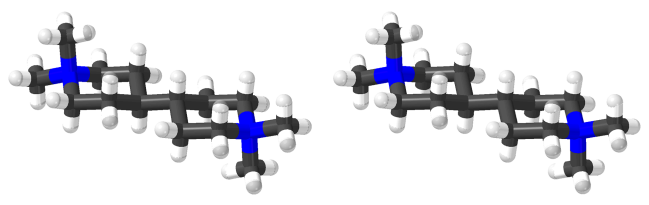


Figure 7. a) ITC thermogram recorded during the competitive titration of a mixture of WP6 (100  $\mu$ M) and G7 (0.2 mM) in the cell with G2 (1.00 mM) in the syringe, b) Fitting of the data to a competitive binding model with  $K_a = 4.59 \times 10^7 \,\mathrm{M}^{-1}$  and  $\Delta H = -6.10 \,\mathrm{kcal}$  mol<sup>-1</sup>.

Measurement of the pK<sub>a</sub> values for WP6. Given the importance of electrostatic interactions on the measured WP6•guest Ka values and the complications likely to be encountered by the computationalists in determining the average charge state of  $\boldsymbol{WP6}$ at neutral pH, we decided to measure the pKa values for WP6. Previously, the Silveira group reported the pKa values for WP5 obtained by pH metric titrations.<sup>19</sup> The authors assume that each portal acts independently and report a total of five pK<sub>a</sub> values: 4.35, 4.49, 4.89. 5.30 and 6.34. Similar pH metric titrations were performed by a contract research organization (Pion, Supporting Information) in three different THF/water mixtures and the pKa values for **WP6** were determined as  $3.62 \pm 0.01$ ,  $4.16 \pm 0.01$ ,  $4.41 \pm$ 0.03, 4.80  $\pm$  0.07, and 5.66  $\pm$  0.01 after extrapolation to pure water using the Yasuda-Shedlovsky equation. Accordingly, WP6 is predominantly present in the dodeca anionic form at pH 7.4

X-ray Crystal Structure of G2. We attempted to grow single crystals of different host•guest complexes of WP6 but were unsuccessful. In one attempt, we obtained single crystals of G2•2l¹ and performed x-ray diffraction measurements and solved the crystal structure of G2 (Figure 8, CCDC 2114714).²0 In brief, guest G2 adopts a linear geometry in the crystal with both dimethyl piperidine rings in the chair conformation. The dihedral angle of the central HC-CH unit of G2 is 180° which minimizes unfavorable gauche butane type interactions.



**Figure 8.** Cross-eyed stereoview of the x-ray crystal structure of **G2**. Color code: C, gray; H, white; N, blue; I, purple.

### Discussion of the Trends in Binding Affinity.

The binding constants measured for the complexation between WP6 and G1 - G17 differ by over five orders of magnitude from 9010  $M^{-1}$  to 4.69 x 10<sup>9</sup>  $M^{-1}$  (Table 1). The WP6•G1 - WP6•G17 complexes all uniformly driven by favorable changes in enthalpy with  $\Delta H$  values ranging from -3.18 kcal mol<sup>-1</sup> for **WP6•G7** to -16.4 kcal mol<sup>-1</sup> for **WP6•G14**. Most of the complexes are also driven by energetically favorable entropic changes with -T∆S values (Supporting Information) ranging from -0.57 kcal mol-1 for WP6•G11 to -4.35 kcal mol<sup>-1</sup> for **WP6•G2** and **WP6•G10**; the **WP6•G1** (+1.63 kcal mol<sup>-1</sup>), WP6•G8 (+3.58 kcal mol<sup>-1</sup>), WP6•G14 (+3.25 kcal mol<sup>-1</sup>), WP6•G16 (+1.87 kcal mol<sup>-1</sup>) complexes are exceptions with positive -T∆S values. These thermodynamic signatures for WP6 guest binding are consistent with the non-classical hydrophobic effect that was established in cyclophane chemistry by Diederich<sup>21</sup> and documented in other systems most notably cucurbiturils.9 Some trends are discernible within this limited dataset and are discussed below.

Influence of the Number of Carbons Among Primary Mono Ammonium Ions. Guests G11 (5 C-atoms), G7 (6 C-atoms), G3 (7 C-atoms), **G6** (8 C-atoms), and **G1** (12 C-atoms) are all primary mono-ammonium ions that differ in the number of Catoms in the hydrophobic residue. The Ka values increase as the number of carbon atoms increases from G11 to G6 which can be explained by the increasing hydrophobicity of the scaffold as CH2 units are incrementally added; we have seen related trends previously with P6AS and CB[n]-type receptors. 14a, 16d, 22 Cyclododecylammonium ion G1 binds more weakly ( $K_a = 5.29 \times 10^4 \text{ M}^{-1}$ ) which suggests that **G1** may be too large for the cavity of **WP6**. Alternatively, the - $T\Delta S$  value for **WP6•G1** is +1.63 kcal mol<sup>-1</sup> which suggests that confinement of the conformationally flexible G1 imposes a large entropic penalty which reduces K<sub>a</sub>. Other primary mono ammoniums whose K<sub>a</sub> values were measured include **G4** and **G9**. Guest **G4** ( $K_a = 5.08 \times 10^4 M^{-1}$ ) which contains one silicon atom was found to bind somewhat more strongly than G11 ( $K_a = 3.37 x$ 

 $10^4~M^{-1}$ ) which can be attributed to the slightly larger volume of **G4** due to the longer C-Si bonds. Adamantane guest **G9** (K<sub>a</sub> = 3.75 x  $10^4~M^{-1}$ ) contains 10 C-atoms but binds even more weakly than **G1** presumably due to the need for the hydrophilic OH functional group of **G9** to remain solvated within the **WP6•G9** complex.

Influence of Guest Charge on Binding Affinity. Diammonium ion guests **G13** ( $K_a = 1.63 \times 10^6 \text{ M}^{-1}$ ), **G10** ( $K_a = 1.61 \times 10^7 \text{ M}^{-1}$ ), **G2** ( $K_a = 4.59 \times 10^7 \text{ M}^{-1}$ ), **G12** ( $K_a = 9.43 \times 10^7 \text{ M}^{-1}$ ), and **G14** ( $K_a = 9.43 \times 10^7 \text{ M}^{-1}$ ), =  $4.69 \times 10^9 \text{ M}^{-1}$ ) are the tighter binders within this dataset. The central hydrophobic cores of G2, G12, and G13 each contain 10 carbon atoms which suggests that the lower Ka measured for G13 is most likely due to the more hydrophilic viologen skeleton. The K<sub>a</sub> for WP6•G13 was previously measured by Huang in less competitive unbuffered water where  $K_a = 1.02 \times 10^8 M^{-1}.^{15}$  Guest **G10** which contains only 8 C-atoms in its central hydrophobic core binds somewhat stronger than G13 but weaker than G2 and (±)-G12. The ability of guests G2, G10, G12, and G13 to engage in favorable ammonium ion • • • carboxylate interactions at both portals of WP6 is likely the source of their high binding affinity. Complex WP6•G14 which is the tightest complex in the dataset two ammonium • • • carboxylate interactions at a single portal (Figure 5).

Cavity size effects. Interestingly, bis quaternary ammonium ion G5 binds very poorly to WP6 (K<sub>a</sub> = 9010 M<sup>-1</sup>) despite its dimethyl adamantane core and its 2+ charge. Figure 9 shows an MMFF minimized molecular model for WP6•G5 which shows that WP6 is too narrow to engulf the hydrophobic core of G5 and instead simply binds to one of the pendant NMe<sub>3</sub><sup>+</sup> groups which explains the especially poor affinity. Related trends have been observed previously by us with CB[n]-type receptors.<sup>8b</sup>

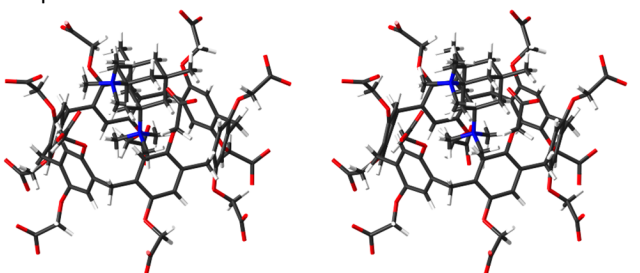


**Figure 9.** Cross-eyed stereoview of an MMFF minimized model of **WP6•G5**. Color code: C, gray; H, white; N, blue; O, red.

Influence of Secondary Electrostatic Interactions. The diammonium ion guests **G2**, **G10**, and **G12** locate their cationic centers near the anionic portals of **WP6**. We wondered about the influence of pendant charged functionality on the observed K<sub>a</sub> values. For example, **G17** is an analogue of **G4** that features a cationic (CH<sub>2</sub>)<sub>3</sub>NH<sub>3</sub><sup>+</sup> sidearm that would be expected to engage in attractive secondary electrostatic interactions with anionic **WP6**. We find that the **WP6•G17** complex is 4.5-fold tighter than the **WP6•G4** complex which corresponds to a difference of -0.89 kcal mol<sup>-1</sup>. Similarly, **G16** 

is an analogue of **G10** that features two anionic (CH<sub>2</sub>)<sub>3</sub>SO<sub>3</sub>-sidearms that would be expected to engage in repulsive secondary electrostatic interactions with anionic **WP6**. Complex **WP6•G16** is 1220-fold weaker than **WP6•G10** which corresponds to a difference of +4.2 kcal mol<sup>-1</sup> (or +2.1 kcal mol<sup>-1</sup> per sidearm). Apparently, repulsive secondary electrostatic interactions exert a larger influence on K<sub>a</sub> that attractive secondary electrostatic interactions.

Influence of Guest Methylation State. In our recent study of **P6AS** we found that higher degrees of guest methylation (e.g.  $1^{\circ} < 2^{\circ} < 3^{\circ} < 4^{\circ}$ ) resulted in significantly higher  $K_a$  values.  $^{14a}$  In the present dataset, p-xylenediamine derived guests **G10** and **G15** differ only in the degree of methylation. We find that the  $K_a$  values for **WP6** toward **G10**  $(1.61 \times 10^7 \ M^{-1})$  and **G15**  $(1.76 \times 10^7 \ M^{-1})$  are quite similar which establishes that methylation state changes do not play a major role in the host•guest trends of **WP6**.

### Conclusions.

In summary, we have reported an investigation of the binding of WP6 toward a panel of cationic hydrophobic guests G1 -**G20** by a combination of <sup>1</sup>H NMR spectroscopy and ITC. The <sup>1</sup>H NMR measurements establish that the hydrophobic binding domains of the guest are located in the hydrophobic cavity of WP6 which constitutes an anisotropic shielding region. The <sup>1</sup>H NMR spectra of WP6•guest complexes may appear simple when guest exchange is fast (e.g. WP6•G1, Figure 3), present a workshop on symmetry considerations when guest exchange is slower (e.g. WP6•G14, Figure 4), or be uninterpretable when WP6 assumes an unsymmetrical conformation (e.g. WP6•G13, Supporting Information). The thermodynamic parameters of binding ( $K_a$ ,  $\Delta H$ ) were measured by direct or competitive ITC and span from a low of 9010 M<sup>-1</sup> for **WP6•G5** to 4.69 x 10<sup>9</sup> M<sup>-1</sup> for WP6•G14. The WP6•guest complexes are generally driven by favorable  $\Delta H$  and less favorable -T $\Delta S$  values which means that the non-classical hydrophobic effect governs the molecular recognition of WP6. The overall guest charge, the number of C-atoms in the hydrophobic binding domain, the presence of secondary electrostatic interactions, and cavity size effects all play a significant role in determining WP6•guest affinity. Perhaps most significantly, thermodynamic data presented in Table 1 serves as a blinded dataset for the SAMPL9 challenge to allow to validate and improve their methods to compute binding free energies in aqueous solution. When those methods reach maturity it will significantly advance wide areas of supramolecular and medicinal chemistry.

### Experimental.

**WP6** was synthesized according to the reported procedure. <sup>15</sup> Guests were available from previous studies. <sup>8, 11b, 11d, 16</sup>  $^{1}$ H NMR spectra were measured on Bruker spectrometers operating at 400 or 600 MHz using D<sub>2</sub>O as solvent. Chemical

Journal Name FULL PAPER

shifts ( $\delta$ ) are referenced relative to the residual resonances for HOD (4.80 ppm). ITC experiments were conducted in the 200  $\mu$ L working volume of the sample cell of a PEAQ ITC instrument (Malvern) using a 40  $\mu$ L injection syringe. Host and guest solutions were prepared in phosphate buffered saline (PBS) at pH 7.4. The sample cell was filled to capacity (200  $\mu$ L) with the host solution and the guest solution was titrated in (first injection = 0.4  $\mu$ L, subsequent 18 injections = 2  $\mu$ L). In select cases, competitive titrations were required where host and an excess of weaker binding guest were included in the cell and the tighter binding guest was titrated into the cell. For direct titrations, the binding data was fitted using the 1:1 binding model implemented in the PEAQ-ITC analysis software whereas for competitive titrations the competition binding model was used.

### Conflicts of Interest.

The authors have no conflicts of interest in relation to the work contained in the paper.

### Acknowledgements.

We thank the National Institutes of Health (GM-124270) and the National Science Foundation (CHE-2105857) for financial support. We thank Profs. Kata Majerski, Marina Sekutor, and Robert Glaser for the samples of **G5**, **G12**, **G19**, and **G20**.

#### **Notes and References**

1 R. C. Mohs and N. H. Greig, *Alzheimers Dement*, 2017, **3**, 651-657. 2 (a) L. Isaacs, SAMPL Challenge,

https://en.wikipedia.org/wiki/SAMPL\_Challenge, (accessed June 11, 2021); (b) H. S. Muddana, C. Daniel Varnado, C. W. Bielawski, A. R. Urbach, L. Isaacs, M. T. Geballe and M. K. Gilson, J. Comput.-Aided Mol. Des., 2012, 26, 475-487; (c) H. S. Muddana, A. T. Fenley, D. L. Mobley and M. K. Gilson, J. Comput.-Aided Mol. Des., 2014, 28, 305-317; (d) J. Yin, N. M. Henriksen, D. R. Slochower, M. R. Shirts, M. W. Chiu, D. L. Mobley and M. K. Gilson, J. Comput.-Aided Mol. Des., 2017, 31, 1-19; (e) A. Rizzi, S. Murkli, J. N. McNeill, W. Yao, M. Sullivan, M. K. Gilson, M. W. Chiu, L. Isaacs, B. C. Gibb, D. L. Mobley and J. D. Chodera, J. Comput.-Aided Mol. Des., 2018, 32, 937-963. 3 (a) M. Isik, D. Levorse, A. S. Rustenburg, I. E. Ndukwe, H. Wang, X. Wang, M. Reibarkh, G. E. Martin, A. A. Makarov, D. L. Mobley, T. Rhodes and J. D. Chodera, J. Comput.-Aided Mol. Des., 2018, 32, 1117-1138; (b) M. Isik, D. Levorse, D. L. Mobley, T. Rhodes and J. D. Chodera, J. Comput.-Aided Mol. Des., 2020, 34, 405-420; (c) D. L. Mobley, S. Liu, N. M. Lim, K. L. Wymer, A. L. Perryman, S. Forli, N. Deng, J. Su, K. Branson and A. J. Olson, J. Comput.-Aided Mol. Des., 2014, 28, 327-345; (d) J. P. Guthrie, J. Phys. Chem. B, 2009, 113, 4501-4507.

4 A. J. Lowe, F. M. Pfeffer and P. Thordarson, *Supramol. Chem.*, 2012, **24**, 585-594.

5 (a) J. M. Dempsey, C. Zhai, H. H. McGarraugh, C. L. Schreiber, S. E. Stoffel, A. Johnson and B. D. Smith, *Chem. Commun.*, 2019, **55**, 12793-12796; (b) K. I. Assaf and W. M. Nau, *Chem. Soc. Rev.*, 2015, **44**, 394-418; (c) Y. Liu, F. Zhou, F. Yang and D. Ma, *Org. Biomol. Chem.*, 2019, **17**, 5106-5111; (d) J. H. Jordan and B. C. Gibb, *Chem. Soc. Rev.*, 2015, **44**, 547-585; (e) A. Bom, M. Bradley, K. Cameron, J.

K. Clark, J. Van Egmond, H. Feilden, E. J. MacLean, A. W. Muir, R. Palin, D. C. Rees and M.-Q. Zhang, *Angew. Chem., Int. Ed.*, 2002, **41**, 265-270; (f) H. Yin, X. Zhang, J. Wei, S. Lu, D. Bardelang and R. Wang, *Theranostics*, 2021, **11**, 1513-1526.

6 (a) W. A. Freeman, W. L. Mock and N.-Y. Shih, *J. Am. Chem. Soc.*, 1981, 103, 7367-7368; (b) J. Kim, I.-S. Jung, S.-Y. Kim, E. Lee, J.-K. Kang, S. Sakamoto, K. Yamaguchi and K. Kim, *J. Am. Chem. Soc.*, 2000, 122, 540-541; (c) A. I. Day, A. P. Arnold, R. J. Blanch and B. Snushall, *J. Org. Chem.*, 2001, 66, 8094-8100; (d) A. I. Day, R. J. Blanch, A. P. Arnold, S. Lorenzo, G. R. Lewis and I. Dance, *Angew. Chem. Int. Ed.*, 2002, 41, 275-277; (e) S. Liu, P. Y. Zavalij and L. Isaacs, *J. Am. Chem. Soc.*, 2005, 127, 16798-16799.

7 (a) S. Ganapati and L. Isaacs, *Isr. J. Chem.*, 2018, **58**, 250-263; (b) L. Isaacs, *Chem. Commun.*, 2009, DOI: 10.1039/b814897j, 619-629. 8 (a) L. Cao, M. Sekutor, P. Y. Zavalij, K. Mlinaric-Majerski, R. Glaser and L. Isaacs, *Angew. Chem. Int. Ed.*, 2014, **53**, 988-993; (b) S. Liu, C. Ruspic, P. Mukhopadhyay, S. Chakrabarti, P. Y. Zavalij and L. Isaacs, *J. Am. Chem. Soc.*, 2005, **127**, 15959-15967.

9 (a) W. M. Nau, M. Florea and K. I. Assaf, *Isr. J. Chem.*, 2011, **51**, 559-577; (b) F. Biedermann, V. D. Uzunova, O. A. Scherman, W. M. Nau and A. De Simone, *J. Am. Chem. Soc.*, 2012, **134**, 15318-15323; (c) F. Biedermann, W. M. Nau and H.-J. Schneider, *Angew. Chem. Int. Ed.*, 2014, **53**, 11158-11171.

10 (a) C.-L. Deng, S. L. Murkli and L. D. Isaacs, *Chem. Soc. Rev.*, 2020, **49**, 7516-7532; (b) H. Jung, K. M. Park, J.-A. Yang, E. J. Oh, D.-W. Lee, K. Park, S. H. Ryu, S. K. Hahn and K. Kim, *Biomaterials*, 2011, **32**, 7687-7694; (c) C. Sun, H. Zhang, S. Li, X. Zhang, Q. Cheng, Y. Ding, L.-H. Wang and R. Wang, *ACS Appl. Mater. Interfaces*, 2018, **10**, 25090-25098; (d) N. J. Wheate and C. Limantoro, *Supramol. Chem.*, 2016, **28**, 849-856.

11 (a) D. Ma, R. Glassenberg, S. Ghosh, P. Y. Zavalij and L. Isaacs, *Supramol. Chem.*, 2012, **24**, 325-332; (b) L. Cao and L. Isaacs, *Supramol. Chem.*, 2014, **26**, 251-258; (c) N. F. She, D. Moncelet, L. Gilberg, X. Y. Lu, V. Sindelar, V. Briken and L. Isaacs, *Chem. Eur. J.*, 2016, **22**, 15270-15279; (d) S. Murkli, J. N. McNeill and L. Isaacs, *Supramol. Chem.*, 2019, **31**, 150-158; (e) S. Z. Ndendjio, W. Liu, N. Yvanez, Z. Meng, P. Y. Zavalij and L. Isaacs, *New J. Chem.*, 2020, **44**, 338-345; (f) S. Murkli, J. Klemm, A. T. Brockett, M. Shuster, V. Briken, M. R. Roesch and L. Isaacs, *Chem. - Eur. J.*, 2021, **27**, 3098-3105.

12 (a) M. R. Sullivan, W. Yao and B. C. Gibb, *Supramol. Chem.*, 2019, **31**, 184-189; (b) P. Suating, T. T. Nguyen, N. E. Ernst, Y. Wang, J. H. Jordan, C. L. D. Gibb, H. S. Ashbaugh and B. C. Gibb, *Chem. Sci.*, 2020, **11**, 3656-3663; (c) K. Kellett, D. R. Slochower, M. Schauperl, B. M. Duggan and M. K. Gilson, *J. Comput.-Aided Mol. Des.*, 2021, **35**, 95-104.

13 (a) M. Xue, Y. Yang, X. Chi, Z. Zhang and F. Huang, *Acc. Chem. Res.*, 2012, **45**, 1294-1308; (b) T. Ogoshi, T.-A. Yamagishi and Y. Nakamoto, *Chem. Rev.*, 2016, **116**, 7937-8002; (c) J.-R. Wu and Y.-W. Yang, *Chem. Commun.*, 2019, **55**, 1533-1543; (d) Z. Li and Y.-W. Yang, *Acc. Mater. Res.*, 2021, **2**, 292-305; (e) X.-Y. Lou and Y.-W. Yang, *Adv. Mater.*, 2020, **32**, 2003263; (f) N. Song, X.-Y. Lou, L. Ma, H. Gao and Y.-W. Yang, *Theranostics*, 2019, **9**, 3075-3093; (g) N. Song, T. Kakuta, T.-A. Yamagishi, Y.-W. Yang and T. Ogoshi, *Chem*, 2018, **4**, 2029-2053.

14 (a) W. Xue, P. Y. Zavalij and L. Isaacs, *Angew. Chem., Int. Ed.*, 2020, **59**, 13313-13319; (b) G. Yu, M. Xue, Z. Zhang, J. Li, C. Han and F. Huang, *J. Am. Chem. Soc.*, 2012, **134**, 13248-13251. 15 G. Yu, X. Zhou, Z. Zhang, C. Han, Z. Mao, C. Gao and F. Huang, *J. Am. Chem. Soc.*, 2012, **134**, 19489-19497. 16 (a) L. Cao, G. Hettiarachchi, V. Briken and L. Isaacs, *Angew.* 

Chem. Int. Ed., 2013, **52**, 12033-12037; (b) L. Cao, D. Skalamera, P.

Y. Zavalij, J. Hostas, P. Hobza, K. Mlinaric-Majerski, R. Glaser and L. Isaacs, *Org. Biomol. Chem.*, 2015, **13**, 6249-6254; (c) D. Sigwalt, M. Sekutor, L. Cao, P. Y. Zavalij, J. Hostas, H. Ajani, P. Hobza, K. Mlinaric-Majerski, R. Glaser and L. Isaacs, *J. Am. Chem. Soc.*, 2017, **139**, 3249-3258; (d) W. Liu, X. Lu, Z. Meng and L. Isaacs, *Org. Biomol. Chem.*, 2018, **16**, 6499-6506.

- 17 H. Zhu, Q. Li, Z. Gao, H. Wang, B. Shi, Y. Wu, L. Shangguan, X. Hong, F. Wang and F. Huang, *Angew. Chem., Int. Ed.*, 2020, **59**, 10868-10872.
- 18 (a) T. Wiseman, S. Williston, J. F. Brandts and L.-N. Lin, *Anal. Biochem.*, 1989, **179**, 131-137; (b) A. Velazquez-Campoy and E. Freire, *Nat. Protocols*, 2006, **1**, 186-191; (c) J. Broecker, C. Vargas and S. Keller, *Anal. Biochem.*, 2011, **418**, 307-309.
- 19 E. V. Silveira, E. H. Wanderlind, A. K. Masson, P. S. Cordeiro, V. Nascimento, R. F. Affeldt and G. A. Micke, *New J. Chem.*, 2020, **44**, 2701-2704.
- 20 Crystal Data for C14H30N2I2 (M =480.20 g/mol): monoclinic, space group P21/c (no. 14), a = 6.5208(2) Å, b = 14.5116(5) Å, c = 10.1283(3) Å,  $\beta$  = 104.2182(5)°, V = 929.05(5) Å3, Z = 2, T = 296(2) K,  $\mu(\text{MoK}\alpha)$  = 3.375 mm-1, Dcalc = 1.717 g/cm3, 16743 reflections measured (5.01°  $\leq$  2  $\Theta$   $\leq$  62.496°), 3037 unique (Rint = 0.0262, Rsig = 0.0147) which were used in all calculations. The final R1 was 0.0240 (I > 2  $\sigma$  (I)) and wR2 was 0.0553 (all data). Refinement details: H atoms were positioned from the geometric considerations and refined as riding on the attached atoms with Uiso constrained to be 20% (50% for methyl group) larger than Ueqv of the attached group. Orientation of methyl groups was optimized. 21 (a) E. A. Meyer, R. K. Castellano and F. Diederich, *Angew. Chem.*,
- 21 (a) E. A. Meyer, R. K. Castellano and F. Diederich, *Angew. Chem., Int. Ed.*, 2003, **42**, 1210-1250; (b) E. Persch, O. Dumele and F. Diederich, *Angew. Chem., Int. Ed.*, 2015, **54**, 3290-3327.
- 22 S. Murkli, J. Klemm, D. King, P. Y. Zavalij and L. Isaacs, *Chem. Eur. J.*, 2020, **26**, 15249-15258.